Piippo, Antti; Hinkkanen, Marko; Luomi, Jorma

Combination of voltage model and high-frequency signal injection for sensorless permanent magnet synchronous motor drives

Published in:
International Conference on Electrical Machines (ICEM'2004)

Published: 05/09/2004

Document Version
Peer-reviewed accepted author manuscript, also known as Final accepted manuscript or Post-print

Combination of Voltage Model and High-Frequency Signal Injection for Sensorless Permanent Magnet Synchronous Motor Drives

A. Piippo, M. Hinkkanen, J. Luomi

Power Electronics Laboratory, Helsinki University of Technology, Finland
P.O. Box 3000, FIN-02015 HUT, Finland, phone: +358 9 4511
e-mail: antti.piippo@hut.fi

Abstract — **The paper proposes a method for the rotor speed and position estimation of permanent magnet synchronous motors, applicable in a wide speed range including standstill. A modified voltage model is used at high speeds, and it is combined with a high-frequency signal injection technique at low speeds. The fast dynamic response of the voltage model is thus augmented with the steady-state accuracy of the high-frequency signal injection technique. The stability and robustness of the combined observer are demonstrated by simulations and experiments.**

I. Introduction

Knowledge of the rotor position is needed for the vector control of a permanent magnet synchronous motor (PMSM). In sensorless control, an estimation algorithm is used instead of a mechanical position sensor, resulting in reduced costs and increased reliability. The methods used for the estimation of the rotor speed and position can be classified into fundamental-excitation methods and signal injection methods.

Fundamental-excitation methods rely on a dynamic model of the motor. The rotor speed and position can be estimated by a voltage model [1] or a more complicated observer [2]–[4]. These methods have good dynamic properties but are not suitable for low-speed operation.

In signal injection methods, a high frequency (HF) voltage signal is superimposed on the stator voltage, and the resulting current response is used for detecting the anisotropy caused by rotor saliency or magnetic saturation [5]–[7]. If persistent HF excitation is applied, the signal is either a revolving voltage vector [6], [7] or a voltage alternating in the estimated rotor reference frame [8]–[10]. The position estimation can be based on a tracking scheme [6], [8]–[10] or on direct evaluation of the rotor position [7], [11], [12]. Signal injection methods work at low speeds and standstill but tend to have restricted dynamic properties.

The methods addressed above have different advantages and disadvantages. Therefore, it would be natural to combine a fundamental-excitation method with a HF signal injection method [13]. Such a combined method has been implemented in sensorless control of induction motors [14]. For PMSMs, a fundamental-excitation method is used at higher speeds and a signal injection method or a combined method at low speeds in [15], [11], [12].

This paper proposes a combined method, in which a modified voltage model is used throughout the whole speed range, and the estimation is augmented with HF signal injection at low speeds. The simple combined method results in good steady-state and dynamic properties over a wide speed range.

II. PMSM Model

The PMSM model is presented in the *d*-*q* reference frame fixed to the rotor. The *d* axis is oriented along the permanent magnet flux, whose angle in the stator reference frame is θ_m in electrical radians. The stator voltage components are

$$u_d = R_s i_d + \frac{d\psi_d}{dt} - \omega_m \psi_q \tag{1a}$$

$$u_q = R_s i_q + \frac{d\psi_q}{dt} + \omega_m \psi_d \tag{1b}$$

where i_d and i_q are the stator current components, R_s is the stator resistance, and $\omega_m = d\theta_m / dt$ is the electrical angular speed of the rotor. The stator flux components are

$$\psi_d = L_d i_d + \psi_{pm} \tag{2a}$$

$$\psi_q = L_q i_q \tag{2b}$$

where L_d and L_q are the *d*- and *q*-axis inductances, respectively, and ψ_{pm} is the permanent magnet flux. The electromagnetic torque is given by

$$T_e = \frac{3}{2} p \left[\psi_{pm} i_q + (L_d - L_q) i_d i_q \right] \tag{3}$$

where p is the number of pole pairs.

III. Observer Structure

A. Modified Voltage Model

The pure voltage model suffers from drift problems due to the open-loop integration. The integration can be replaced by low-pass filtering and error compensation [16], [17].

The modified voltage model in the estimated rotor reference frame is formed from (1) and (2) as

$$\frac{d\hat{\psi}_{pm}}{dt} = \hat{e}_d + \alpha_v (\psi_{pm0} - \hat{\psi}_{pm}) \tag{4a}$$

$$\hat{\omega}_m = \frac{\hat{e}_q}{\hat{\psi}_{pm}} \tag{4b}$$

where the estimates of the back-emf components are

$$\hat{e}_d = u_d - \hat{R}_s i_d - \hat{L}_d \frac{di_d}{dt} + \hat{\omega}_m \hat{L}_q i_q \tag{5a}$$

$$\hat{e}_q = u_q - \hat{R}_s i_q - \hat{L}_q \frac{di_q}{dt} - \hat{\omega}_m \hat{L}_d i_d \tag{5b}$$

Estimates are marked by the symbol ˆ, ψ_{pm0} is the presumed value of the permanent magnet flux, and α_v is a nonnegative gain. Furthermore, the estimate of the rotor position is obtained by integrating $\hat{\omega}_m$. The pure voltage model is obtained by choosing $\alpha_v = 0$. For $\alpha_v > 0$, the open-loop integrator is replaced with a low-pass filter having the bandwidth of α_v, and the error so introduced is compensated using ψ_{pm0}.

B. High-Frequency Signal Injection

An alternating voltage is used for HF signal injection [8]–[10]. A carrier excitation signal fluctuating at angular frequency ω_c and having amplitude $\hat{u}_c$, i.e.,

$$u_c = \hat{u}_c \cos(\omega_c t) \tag{6}$$

is superimposed on the *d* component of the stator voltage in the estimated rotor reference frame. An HF current response is detected in the *q* direction of the estimated rotor reference frame, amplitude modulated by the rotor position estimation error. The principle of the demodulation scheme is shown in Fig. 1. The *q* component of the measured current is band-pass filtered (BPF), giving the current signal i_{qc} varying at the signal injection frequency. The current signal is then demodulated and low-pass filtered (LPF) to extract an error signal

$$\varepsilon = \mathrm{LPF}\{i_{qc} \sin(\omega_c t)\} \tag{7}$$

Ideally, this error signal is [8]

$$\varepsilon = \underbrace{\frac{\hat{u}_c}{\omega_c} \frac{L_q - L_d}{4 L_q L_d}}_{K_\varepsilon} \sin(2\tilde{\theta}_m) \tag{8}$$

where K_ε is the signal injection gain and $\tilde{\theta}_m = \theta_m - \hat{\theta}_m$ is the estimation error of the rotor position.

The demodulation scheme is implemented as follows. Instead of using a band-pass filter, the filtering of i_q is achieved by

$$i_{qc} = i_q - \frac{1}{T_c} \int_{t-T_c}^{t} i_q dt \tag{9}$$

where $T_c = 2\pi / \omega_c$, i.e. by zero averaging over one period of the injection signal. The algorithm (9) can be interpreted as a high-pass filter, and its computational cost is lower than that of relevant band-pass filters. The low-pass filtering of the signal $i_{qc} \sin(\omega_c t)$ is implemented using two filters: a moving-average filter and a first-order low-pass filter. The moving-average filter removes the angular frequency ω_c and its multiples effectively and causes only a short time delay, while the first-order low-pass filter reduces stochastic noise more effectively than the moving-average filter. Due to the short delay of the moving-average filter, only the dynamics of the first-order low-pass filter are considered in the following. After filtering, the amplitude of ε is limited to avoid errors during transients.

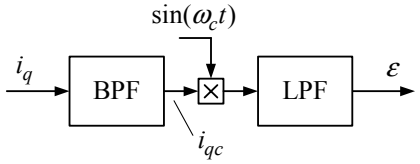

Figure 1. Principle of error signal demodulation.

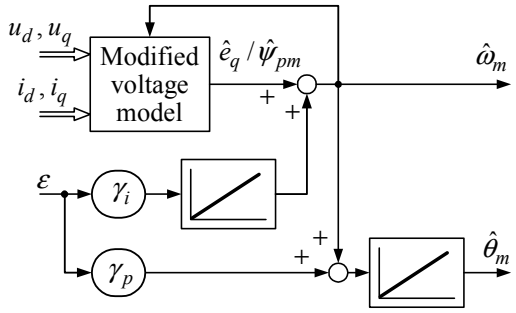

Figure 2. Block diagram of the combined observer.

C. Combined Observer

The combination of the modified voltage model and the HF signal injection method is illustrated in Fig. 2. The rotor speed and position estimates are obtained by

$$\hat{\omega}_m = \frac{\hat{e}_q}{\hat{\psi}_{pm}} + \gamma_i \int \varepsilon \, dt \tag{10a}$$

$$\hat{\theta}_m = \int (\hat{\omega}_m + \gamma_p \varepsilon) \, dt \tag{10b}$$

where γ_p and γ_i are positive gains, $\hat{\psi}_{pm}$ is estimated using (4a), and $\hat{e}_d$ and $\hat{e}_q$ (5) are evaluated using $\hat{\omega}_m$ from (10a). The HF signal injection and a phase-locked loop (PLL) [13], [9] are used to augment the speed estimate obtained by the modified voltage model. The PI mechanism in (10) drives the error signal ε to zero in steady state. At low speeds, the combined observer relies both on the signal injection method and the voltage model: the signal injection method dominates in steady state whereas the voltage model commands at transients.

The PI mechanism used in a PLL can be tuned analytically [9]. The transfer function $\hat{\theta}_m(s) / \theta_m(s)$, corresponding to the linearized closed-loop system shown in Fig. 3, can be used for determining the gains γ_p and γ_i. From (8), a linear approximation

$$\varepsilon \approx 2 K_\varepsilon \tilde{\theta}_m \tag{11}$$

is used when determining the closed-loop transfer function. The influence of the voltage model is omitted, but the low-pass filter used in (7) is taken into account. The transfer function of the first-order low-pass filter having the bandwidth α_{lp} is

$$F(s) = \frac{\alpha_{lp}}{s + \alpha_{lp}} \tag{12}$$

and the transfer function of the PI mechanism is

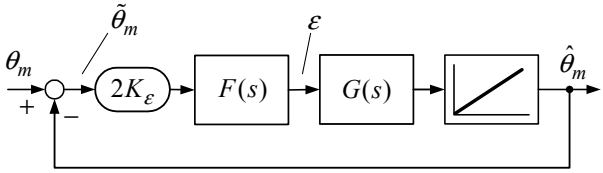

Figure 3. Block diagram of the closed-loop system.

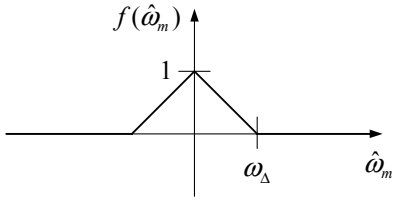

Figure 4. Dependence of signal injection amplitude and PLL bandwidth on rotor speed.

$$G(s) = \gamma_p + \frac{\gamma_i}{s} \tag{13}$$

For the closed-loop system in Fig. 3, the transfer function is

$$\frac{\hat{\theta}_m(s)}{\theta_m(s)} = \frac{2K_\varepsilon\alpha_{lp}\gamma_p s + 2K_\varepsilon\alpha_{lp}\gamma_i}{s^3 + \alpha_{lp}s^2 + 2K_\varepsilon\alpha_{lp}\gamma_p s + 2K_\varepsilon\alpha_{lp}\gamma_i} \tag{14}$$

To ensure stability and to avoid oscillations, all three poles of (14) are placed to the point $-\alpha$ on the real axis yielding the selection rule

$$\alpha_{lp} = 3\alpha \tag{15}$$

for the low-pass filter bandwidth and the selection rules

$$\gamma_p = \frac{\alpha}{2K_\varepsilon}, \qquad \gamma_i = \frac{\alpha^2}{6K_\varepsilon} \tag{16}$$

for the gains of the PI mechanism. The proposed design method allows gain selection using only one design parameter α corresponding to the approximate bandwidth of the closed-loop system (14).

In order to obtain a smooth transition between the low-speed and high-speed regions, the injection voltage amplitude $\hat{u}_c$ and the bandwidth α are decreased linearly with increasing speed, and the signal injection is disabled above transition speed ω_Δ, i.e.,

$$\hat{u}_c = f(\hat{\omega}_m)\,\hat{u}_{c0}, \qquad \alpha = f(\hat{\omega}_m)\,\alpha_0 \tag{17}$$

where $\hat{u}_{c0}$ and α_0 are the values corresponding to zero-speed operation and function $f(\hat{\omega}_m)$ is shown graphically in Fig. 4. The parameters α_{lp} and γ_i are varied according to (15), (16), and (8). The parameter γ_p remains constant according to (16) and (8).

IV. Control System

The block diagram of the control system comprising cascaded speed and current control loops is shown in Fig. 5. The current control is implemented as PI-type control in the estimated rotor reference frame, where the cross-coupling terms and the back-emf are decoupled [18].

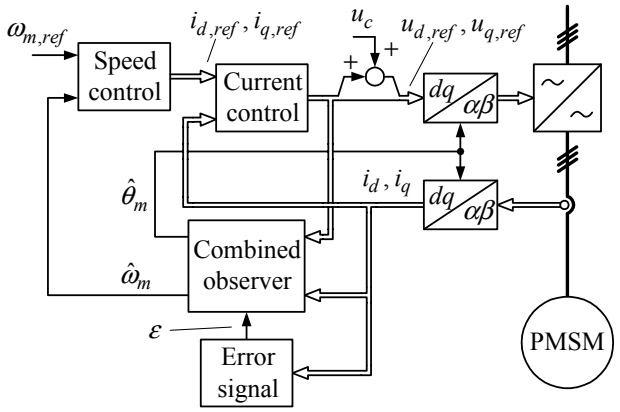

Figure 5. Block diagram of the control system.

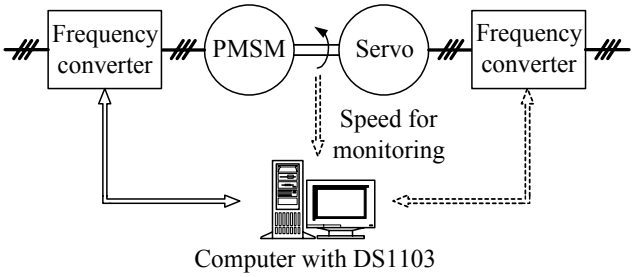

Figure 6. Experimental setup. Mechanical load is provided by the servo drive.

PI-type speed control with active damping is used. The current references $i_{d,ref}$ and $i_{q,ref}$ are calculated according to maximum torque per current control [19]. The dc-link voltage of the converter is measured, and simple current feedforward dead-time compensation is applied [20].

V. Results

The proposed observer was investigated by means of simulations and laboratory experiments. The experimental setup is illustrated in Fig. 6. A 2.2-kW internal-magnet PMSM is fed by a frequency converter controlled by a dSPACE DS1103 PPC/DSP board. The base values and the motor parameters are given in Table I and the parameters of the control system in Table II. The sampling is synchronized to the modulation, and both the switching frequency and the sampling frequency are 5 kHz. The dc-link voltage is 540 V. The signal injection frequency is 500 Hz, and the transition speed $\omega_\Delta = 0.13$ p.u. At zero speed, the amplitude of the HF voltage signal is $\hat{u}_{c0} = 20$ V, and the measured rms value of the HF current is 190 mA, i.e. 0.04 p.u. The electromagnetic torque is limited to 22 Nm, i.e. $T_{max}/T_N = 1.57$. An incremental encoder is used to monitor the actual rotor speed and position, which is further used to calculate the rotor position estimation error.

The MATLAB/Simulink environment was used for the simulations. The parameters of the motor model used in the simulations correspond to the parameters of the motor

TABLE I. MOTOR DATA

Nominal power	2.2 kW
Nominal/base voltage	370 V
Nominal/base current	4.3 A
Nominal/base frequency	75 Hz
Nominal speed	1500 r/min
Nominal torque T_N	14.0 Nm
Number of pole pairs p	3
Stator resistance R_s	4.10 Ω
Direct axis inductance L_d	0.036 H
Quadrature axis inductance L_q	0.051 H
Permanent magnet flux ψ_{pm}	0.545 Vs
Total moment of inertia	0.015 kgm^2

TABLE II. CONTROL SYSTEM PARAMETERS

Signal injection amplitude $\hat{u}_c$	20 V
Signal injection angular frequency ω_c	2π500 rad/s
Bandwidth α_0	2π10 rad/s
Voltage model gain α_v	2π15 rad/s
Current controller bandwidth	2π200 rad/s
Speed controller bandwidth	2π2.5 rad/s

used in the experiments. In the simulations, white noise having an rms value of 10 mA was added to the measured phase currents of the motor, and the current signals were quantized in steps of 10 mA.

Figs. 7−9 show simulation results during a slow speed reversal at nominal load torque. The speed reference was changed linearly from 0.2 p.u. to −0.2 p.u. between $t = 2$ s and $t = 28$ s. The stator resistance estimate $\hat{R}_s$ is accurate in Fig. 7, whereas the stator resistance is 10 % underestimated in Fig. 8 and 10 % overestimated in Fig. 9. The results show that a parameter error causes an orientation error, but at low speeds, the signal injection technique nearly removes the estimation error of the rotor position. The transition between the voltage model and the combined observer is smooth, and the speed estimate follows the actual speed with a good accuracy although a parameter error is present.

Fig. 10 shows experimental results during the slow speed reversal at nominal load torque. The results show stable operation both in the motoring and regenerating modes. Furthermore, it can be seen that the experimental results correspond well to the simulation results. At low speeds, however, the rotor position estimation error varies more in the experimental results than in the simulation results. This ripple consists mostly of a sixth harmonic component. Therefore, proper compensation of inverter nonlinearities is a suitable topic of future research.

Fig. 11 shows experimental results at no load when the speed reference was changed stepwise from zero to 0.2 p.u. at $t = 1$ s, then reversed to −0.2 p.u. at $t = 2$ s, and finally set to zero at $t = 3$ s. The estimated rotor speed follows the actual speed smoothly and the rotor position estimation error stays in reasonable small values.

Fig. 12 depicts experimental results when the speed reference was set to zero. The load torque was first changed stepwise from zero to the nominal value at $t = 1$ s, then reversed at $t = 2$ s, and removed at $t = 3$ s. The error

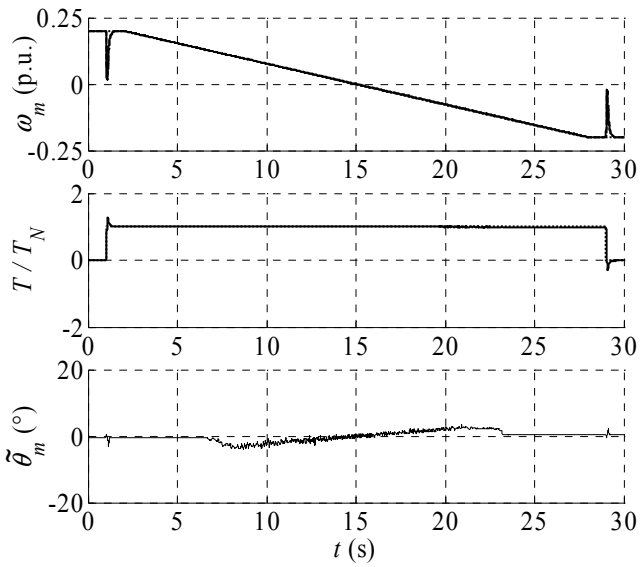

Figure 7. Simulation results showing slow speed reversal at nominal load torque, $\hat{R}_s = R_s$. First subplot shows electrical angular speed (solid), its estimate (dashed), and its reference (dotted). Second subplot shows estimated electromagnetic torque (solid) and load torque reference (dotted). Last subplot shows estimation error of rotor position in electrical degrees.

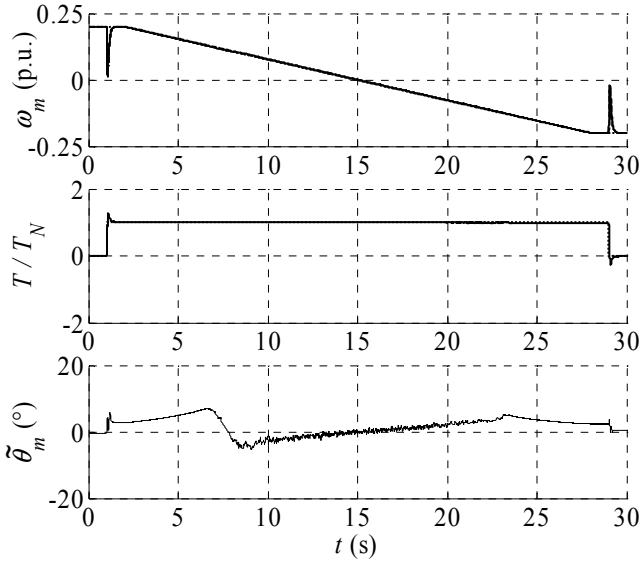

Figure 8. Simulation results showing slow speed reversal at nominal load torque, $\hat{R}_s = 0.9R_s$. Explanations of the curves are as in Fig. 7.

of the rotor position estimate is small even during transients, indicating good dynamic performance.

Experimental results at the nominal load torque are shown in Fig. 13. The speed reference was first changed stepwise from zero to 0.66 p.u. at $t = 1$ s, then reversed to −0.66 p.u. at $t = 2$ s, and finally set to zero at $t = 3$ s. The estimated rotor speed follows the actual speed smoothly even during the transitions between the voltage model and the combination of the voltage model and HF signal injection.

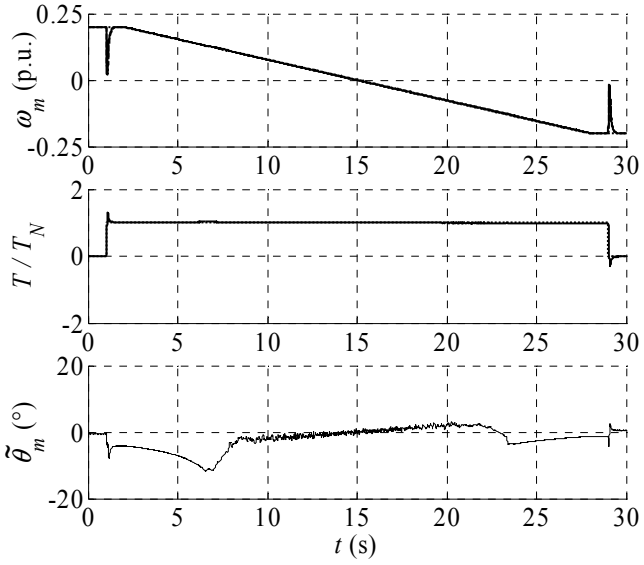

Figure 9. Simulation results showing slow speed reversal at nominal load torque, $\hat{R}_s = 1.1R_s$. Explanations of the curves are as in Fig. 7.

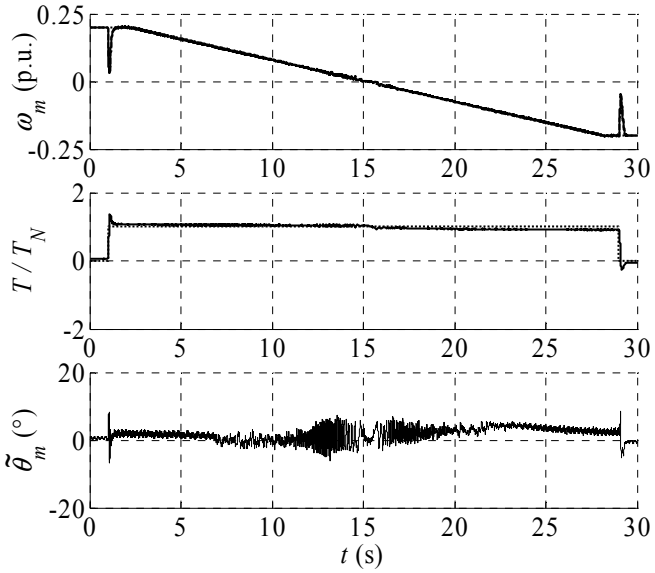

Figure 10. Experimental results showing slow speed reversal at nominal load. Explanations of the curves are as in Fig. 7.

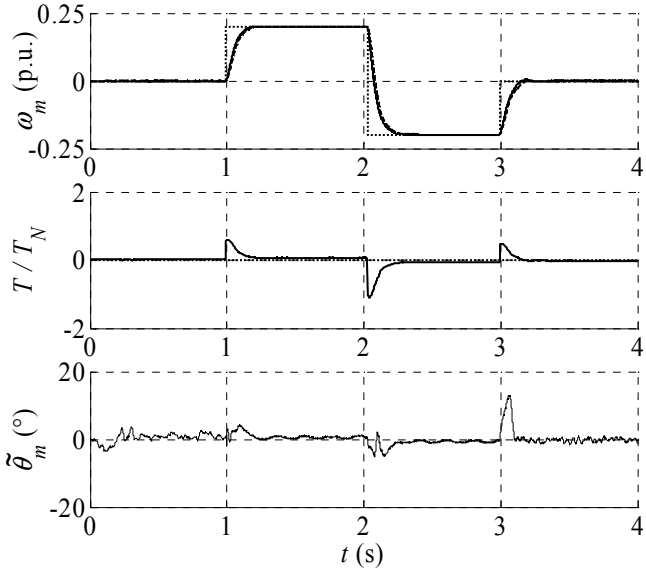

Figure 11. Experimental results showing speed reference steps at zero load torque. Explanations of the curves are as in Fig. 7.

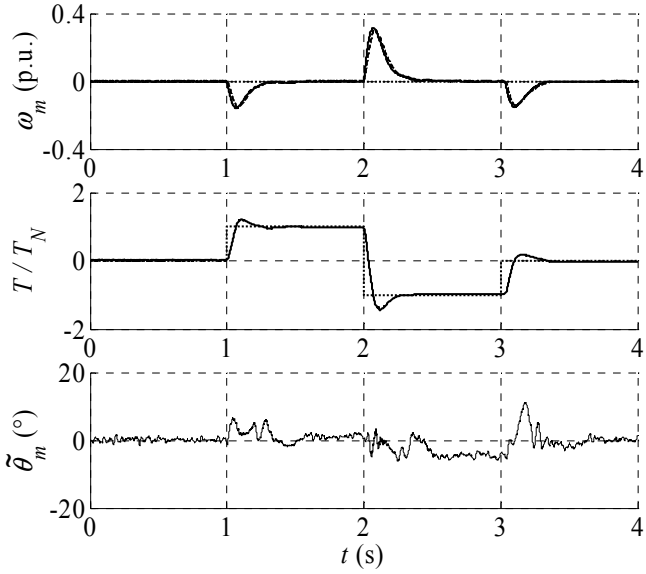

Figure 12. Experimental results showing load torque steps at zero speed reference. Explanations of the curves are as in Fig. 7.

VI. CONCLUSIONS

A modified voltage model that is augmented with a high-frequency signal injection technique at low speeds is suitable for the estimation of the rotor speed and position of a permanent magnet synchronous motor in a wide speed range, including zero speed. The fast dynamic response of the voltage model is combined with the steady-state accuracy of the high-frequency signal-injection method. The signal injection scheme is based on a voltage carrier signal alternating in the estimated rotor reference frame and simple demodulation of the current response. Guidelines for the gain selection of the tracking observer are obtained analytically. According to the simulations and experiments presented in the paper, the system based on the combined observer is stable and robust, and can cope with stepwise changes in the speed reference and with nominal load torque steps.

ACKNOWLEDGEMENT

The authors gratefully acknowledge the financial support given by ABB Oy and the Finnish Cultural Foundation.

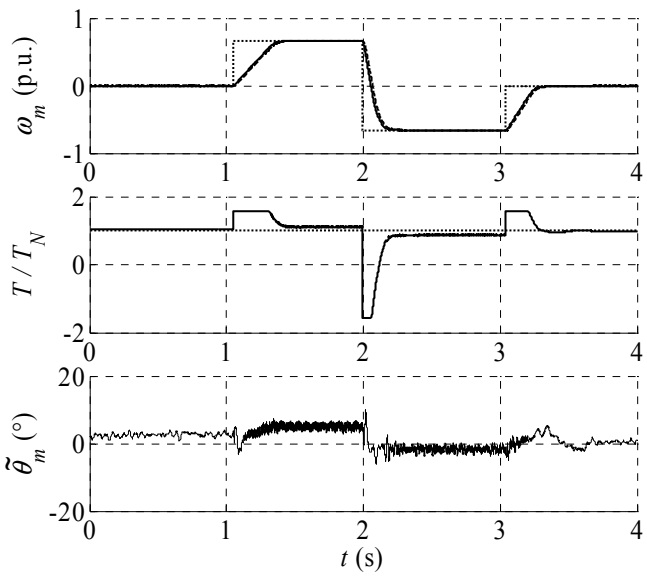

Figure 13. Experimental results showing speed reference steps at nominal load. Explanations of the curves are as in Fig. 7.

REFERENCES

[1] R. Wu and G. R. Slemon, "A permanent magnet motor drive without a shaft sensor," *IEEE Trans. Ind. Applicat.*, vol. 27, no. 5, pp. 1005–1011, Sept./Oct. 1991.

[2] R. B. Sepe and J. H. Lang, "Real-time observer-based (adaptive) control of a permanent-magnet synchronous motor without mechanical sensors," *IEEE Trans. Ind. Applicat.*, vol. 28, no. 6, pp. 1345–1352, Nov./Dec. 1992.

[3] J. Solsona, M. I. Valla, and C. Muravchik "A nonlinear reduced order observer for permanent magnet synchronous motors," *IEEE Trans. Ind. Electron.*, vol. 43, no. 4, pp. 492–497, Aug. 1996.

[4] S. Bolognani, R. Oboe, and M. Zigliotto, "Sensorless full-digital PMSM drive with EKF estimation of speed and rotor position," *IEEE Trans. Ind. Electron.*, vol. 46, no. 1, pp. 184–191, Feb. 1999.

[5] M. Schroedl, "Sensorless control of AC machines at low speed and standstill based on the "INFORM" method," in *Conf. Rec. IEEE-IAS Annu. Meeting*, vol. 1, San Diego, CA, Oct. 1996, pp. 270–277.

[6] P. L. Jansen and R. D. Lorenz, "Transducerless position and velocity estimation in induction and salient AC machines," *IEEE Trans. Ind. Applicat.*, vol. 31, no. 2, pp. 240–247, March/April 1995.

[7] A. Consoli, G. Scarcella, and A. Testa, "Industry application of zero-speed sensorless control techniques for PM synchronous motors," *IEEE Trans. Ind. Applicat.*, vol. 37, no. 2, pp. 513–521, March/April 2001.

[8] M. Corley and R. D. Lorenz, "Rotor position and velocity estimation for a salient-pole permanent magnet synchronous machine at standstill and high speeds," *IEEE Trans. Ind. Applicat.*, vol. 43, no. 4, pp. 784–789, July/Aug. 1998.

[9] L. Harnefors and H.-P. Nee, "A general algorithm for speed and position estimation of AC motors," *IEEE Trans. Ind. Electron.*, vol. 47, no. 1, pp. 77–83, Feb. 2000.

[10] M. Linke, R. Kennel, and J. Holtz, "Sensorless position control of permanent magnet synchronous machines without limitation at zero speed," in *Proc. IEEE IECON'02*, vol. 1, Sevilla, Spain, Nov. 2002, pp. 674–679.

[11] C. Silva, G. M. Asher, and M. Sumner, "An hf signal-injection based observer for wide speed range sensorless PM motor drives including zero speed," in *Proc. EPE'03*, vol. 1, Toulouse, France, Sept. 2003, pp. 1–9.

[12] M. Tursini, R. Petrella, and F. Parasiliti, "Sensorless control of an IPM synchronous motor for city-scooter applications," in *Conf. Rec. IEEE IAS Annu. Meeting*, vol. 3, Salt Lake City, UT, Oct. 2003, pp. 1472– 1479.

[13] P. L. Jansen, M. J. Corley, and R. D. Lorenz, "Flux, position, and velocity estimation in ac machines at zero and low speed via tracking of high frequency saliencies," in *Proc. EPE'95*, vol. 3, Sevilla, Spain, Sept. 1995, pp. 154–159.

[14] K. Ide, J.-I. Ha, M. Sawamura, H. Iura, and Y. Yamamoto, "A novel hybrid speed estimator of flux observer for induction motor drives," in *Proc. IEEE ISIE'02*, vol. 3, L'Aquila, Italy, July 2002, pp. 822–827.

[15] E. Robeischl, M. Schroedl, and M. Krammer, "Position-sensorless biaxial position control with industrial PM motor drives based on INFORM- and back EMF model," in *Proc. IEEE IECON'02*, vol. 1, Sevilla, Spain, Nov. 2002, pp. 668–673.

[16] T. Ohtani, N. Takada, and K. Tanaka, "Vector control of induction motor without shaft encoder," *IEEE Trans. Ind. Applicat.*, vol. 28, no. 1, pp. 157–164, Jan./Feb. 1992.

[17] H. Rasmussen, P. Vadstrup, and H. Børsting, "Sensorless field oriented control of a pm motor including zero speed," in *Proc. IEEE IEMDC'03*, vol. 2, Madison, WI, June. 2003, pp. 1224–1228.

[18] F. Briz del Blanco, M. W. Degner, and R. D. Lorenz, "Dynamic analysis of current regulators for AC motors using complex vectors," *IEEE Trans. Ind. Applicat.*, vol. 35, no. 6, pp. 1424–1432, Nov./Dec. 1999.

[19] T. Jahns, G. Kliman, and T. Neumann, "Interior permanent-magnet synchronous motors for adjustable-speed drives," *IEEE Trans. Ind. Applicat.*, vol. 22, no. 4, pp. 738–747, July/Aug. 1986.

[20] J. K. Pedersen, F. Blaabjerg, J. W. Jensen, and P. Thogersen, "An ideal PWM-VSI inverter with feedforward and feedback compensation," in *Proc. EPE'93*, vol. 5, Brighton, UK, Sept. 1993, pp. 501–507.